Modeling of Path Arrival Rate for In-Room Radio Channels With Directive Antennas

Pedersen, Troels

Published in:
IEEE Transactions on Antennas and Propagation

DOI (link to publication from Publisher):
10.1109/TAP.2018.2846785

Publication date:
2018

Document Version
Accepted author manuscript, peer reviewed version

This article has been accepted for publication in a future issue of this journal, but has not been fully edited. Content may change prior to final publication. Citation information: DOI 10.1109/TAP.2018.2846785, IEEE Transactions on Antennas and Propagation

Modelling of Path Arrival Rate for In-Room Radio Channels with Directive Antennas

Troels Pedersen

***Abstract*—We analyze the path arrival rate for an inroom radio channel with directive antennas. The impulse response of this channel exhibits a transition from early separate components followed by a diffuse reverberation tail. Under the assumption that the transmitter's (or receiver's) position and orientation are picked uniformly at random we derive an exact expression of the mean arrival rate for a rectangular room predicted by the mirror source theory. The rate is quadratic in delay, inversely proportional to the room volume, and proportional to the product of beam coverages of the transmitter and receiver antennas. Making use of the exact formula, we characterize the onset of the diffuse tail by defining a "mixing time" as the point in time where the arrival rate exceeds one component per transmit pulse duration. We also give an approximation for the power-delay spectrum. It turns out that the power-delay spectrum is unaffected by the antenna directivity. However, Monte Carlo simulations show that antenna directivity does indeed play an important role for the distribution of instantaneous mean delay and rms delay spread.**

***Index Terms*—Radio propagation, indoor environments, reverberation, room electromagnetics.**

I. Introduction

Stochastic multipath models for the channel impulse response are useful tools for the design, analysis and simulation of systems for radio localization and communications. These models allow for tests via Monte Carlo simulation and in many cases provide analytical results useful for system design. Many such models exist for the complex baseband representation of the signal at the receiver antenna[1]

$$y(\tau) = \sum_k \alpha_k s(\tau - \tau_k), \tag{1}$$

term k has delay τ_k and complex gain α_k corresponding to path k and $s(\tau)$ is the complex baseband representation of the transmitted signal [1]. The gains and delays form a marked point process with points $\{\tau_k\}$ and marks $\{\alpha_k\}$. The arrival process $\{\tau_k\}$ has an intensity function $\lambda(\tau)$ referred to as the (path) arrival rate [2]. A particularly prominent example is the model by Turin [2] where the delays are drawn from a Poisson point process. Although Turin's model was originally intended for urban radio channels, it has since been taken as basis for a wide range of models for outdoor and indoor channels including the models by, Suzuki [3], Hashemi [4], Saleh and Valenzuela [5], Spencer et al. [6] and Zwick et al. [7], [8]. More recently, this type of statistical channel models has been considered for the millimeter-wave applications [9], [10].

For a model to be trustworthy its parameter settings should be properly chosen. Empirical parameter estimation methods are wide-spread in the literature. Indeed, Turin along with the scientists elaborating this modeling approach [3]–[10] determined the parameters based on measurements. The empirical approach, however, gives only limited insight into how model parameters vary with the propagation environment or system parameters such as frequency bands and antenna configurations. Therefore, costly measurement campaigns performed for one particular type of environment and radio system may have to be redone in case the model should be adapted to a different situation, e.g. if considering new frequency bands or different antenna configurations. A further complications comes from the fact that, the model in (1) is unidentifiable in the power-delay spectrum. To see this, observe that for the most often considered case of uncorrelated zero mean gains, the second moment of the received signal reads

$$\mathbb{E}[|y(\tau)|^2] = \int_{-\infty}^{\infty} P(\tau - t)|s(t)|^2 dt, \tag{2}$$

where the power-delay spectrum, $P(\tau)$, is a product

$$P(\tau) = \sigma_\alpha^2(\tau)\lambda(\tau), \tag{3}$$

with $\sigma_\alpha^2(\tau)$ denoting the variance of a complex gain at a given delay. According to (3), exactly the same delay-power spectrum can be obtained by a continuum of combinations of arrival rates and conditional mark variances. This effect is clearly present for Turin's model, but as noted in [11], also holds true for the Saleh-Valenzuela model [5]: by interchanging inter- and intra-cluster parameters for rates and complex gains, and thereby completely altering the model's behaviour, the same power-delay spectrum is obtained. If two of the three entities related through (3), are specified, the third can be determined.

As a much less explored alternative to the empirical approach, model parameters can in some cases be obtained by analysis of the propagation environment. Potentially, this analytical approach allows us to predict how changes in the propagation environment or in system parameters will affect the channel model parameters. Unfortunately, most realistic propagation environments are too complex to permit such analysis and therefore, we can at best hope to analyze simplistic, but elemental, scenarios. Such elemental results may help us to better understand more realistic scenarios.

June 8, 2018, This work is supported by the Cooperative Research Project VIRTUOSO, funded by Intel Mobile Communications, Keysight, Telenor, Aalborg University, and the Danish National Advanced Technology Foundation. This work was performed within the framework of the COST Action CA15104 IRACON. T. Pedersen is with the Department of Electronic Systems, Section Wireless Communication Networks, Aalborg University, Aalborg, 9220, Denmark (e-mail: troels@es.aau.dk).

[1]Here we omit any additive terms due to noise or interference as our focus is on characterizing the contribution related to the transmitted signal.

This article has been accepted for publication in a future issue of this journal, but has not been fully edited. Content may change prior to final publication. Citation information: DOI 10.1109/TAP.2018.2846785, IEEE Transactions on Antennas and Propagation

The elemental case where one transmitter and one receiver sit in the same rectangular room has been studied in a number of works [12]–[17] using the theory of room electromagnetics. These investigations have focused on determining the reverberation time which characterizes the exponentially decaying reverberation tail of the average power-delay profile, or power-delay spectrum. Room electromagnetics has also been considered as a means to set the parameters of other models through entities derived from the power-delay spectrum [18]–[20].

Models for the delay power spectrum have been studied intensively in the room electromagnetics literature, e.g. [12]–[17]. Most attention has been devoted to modeling the reverberation time which specifies the decay of the power delay spectrum. The model by Sabine [21] appears to be the most popular, see e.g. [13]–[17]. However, Eyring's model [22], first used for room electromagnetics in [12], predicts the reverberation time more accurately [17]. Interestingly, in the process of deriving the reverberation time using an approximation based on mirror source theory, Eyring actually derived an approximation for the arrival rate at large delays for a rectangular room using mirror source theory. According to Eyring's approximation the arrival rate increases quadratically with delay and is inversely proportional to the room volume. Thereby this model captures a transition effect of the received signal from early specular contributions to the late diffuse reverberation tail, similar to the effect considered for in-room radio propagation [23]–[27].

The contributions of the present paper is to adapt Eyring's analysis to radio channel modeling by including antenna positions, orientations, and antenna directivity. The effect of the antenna directivity on the "richness" of measured impulse responses has been noticed qualitatively in early measurements [28] and the impact of antenna directivity on small scale fading parameters has been studied in several works [29]–[31]. Our approach leads to an exact expression for the mean arrival rate for the mirror source model; for special cases our expression coincide with Eyring's approximation. The rate is quadratic in delay, inversely proportional to the room volume, and proportional to the product of beam coverages of the transmitter and receiver antennas. Making use of the exact formula, we characterize the onset of the diffuse tail by defining a "mixing time". We also give an approximation for the power-delay spectrum and study the mean delay and rms delay spread via simulations. It turns out that the power-delay spectrum is unaffected by the antenna directivity, while the mean delay and rms delay spread vary.

We proceed in Section II by introducing the rectangular room considering non-isotropic antennas for which Section III details the mirror source theory. In Section IV, we develop an approximation for the arrival rate of this model with deterministic antenna positions and orientations. In Section V, we analyze the mean arrival rate for random transmitter position and antenna orientation. An expression for power delay spectrum is developed in Section VI. In Section VII, we illustrate the results of the analysis by Monte Carlo simulations. Discussion and conclusions are given in Sections VIII and IX.

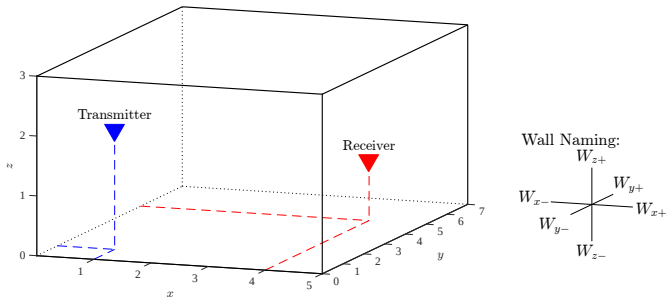

Fig. 1. Three-dimensional rectangular room with transmitter and receiver inside along with the coordinate system and wall naming convention.

II. Rectangular Room With Directive Antennas

Consider a rectangular room illustrated in Fig. 1 with directional transmitter and receiver antennas located inside. Throughout the paper, entities related to the transmitter and receiver have subscripts T and R respectively. The room is of dimension $L_x \times L_y \times L_z$ and has volume $V = L_x L_y L_z$. The room has six walls (including floor and ceiling). The two walls parallel to the yz-plane are denoted by W_{x-}, for the left-most wall (with $x = 0$) and W_{x+} for the rightmost wall (with $x = L_x$). Similarly, we refer to the remaining walls as respectively W_{y-}, W_{y+}, W_{z-}, and W_{z+}. We assume that the carrier wavelength l_c is small compared to the room dimensions, and that only specular reflections occur with a gain independent of incidence direction. The power gain (or reflectance) of wall i is denoted by g_i. Positions are given with reference to a Cartesian coordinate system with origin at one corner and aligned such that the room spans the set $[0, L_x) \times [0, L_y) \times [0, L_z)$. Then the positions of the transmitter and receiver are given as $r_T = [x_T, y_T, z_T]^T$ and $r_R = [x_R, y_R, z_R]^T$.

The antennas are both assumed to be directive and their radiation patterns can have strong back- and side-lobes. To describe the antennas, we follow the IEEE standard terminology as defined in [32]. For simplicity reason, we ignore polarization, and thus describe the antennas only by their gain. The antenna gain in the direction specified by the 3-dimensional real unit vector Ω by $G(\Omega)$ (power per solid angle). The forthcoming analysis does not change substantially by considering lossy antennas, and we therefore consider only lossless antennas. Then the integral of the antenna gain over the sphere equals 4π. We remark that the equations can be readily adapted by including the radiation efficiency in equations where the antenna gain enters.

It is customary to describe a directive antenna by its beamwidth or its maximum gain $G_{\max} = \max_\Omega G(\Omega)$. However, these characteristics only describes the mainlobe and are blind to the presence of side-lobes. Instead we use another standardized characteristic, namely the footprint of the antenna [32] on a unit sphere centered at the antenna. We may think of the foot print as the portion of the sphere "illuminated by the antenna". The footprint denoted by $\mathcal{O}$ can be mathematically defined as the set

$$\mathcal{O} = \{\Omega : G(\Omega) \geq \epsilon \cdot G_{\max}\}, \tag{4}$$

This article has been accepted for publication in a future issue of this journal, but has not been fully edited. Content may change prior to final publication. Citation information: DOI 10.1109/TAP.2018.2846785, IEEE Transactions on Antennas and Propagation

where $\epsilon \geq 0$ specifies a gain level below which, the gain of the antenna is considered insignificant. The appropriate value for ϵ may vary with application in mind. In the present work we shall not be concerned with the particular value of ϵ, but assume it small. The size of the footprint is the called the beam coverage solid angle [32] measured in steradians as

$$|\mathcal{O}| = \int_{\mathbb{S}_2} \mathbb{1}(\Omega \in \mathcal{O}) d\Omega. \tag{5}$$

Here, $\mathbb{S}_2$ is the unit sphere and $\mathbb{1}(\cdot)$ denotes an indicator function with value one if the argument is true and zero otherwise. The beam coverage can (upon specification of ϵ) be computed for a given gain pattern according to (4) and (5). It measures the total solid angle of the main- and sidelobes of the gain pattern. With this definition, the beam coverage solid angle ranges from zero to 4π steradians. Although the beam coverage solid angle is a standardized term [32], it is not a widely used antenna characteristic. We use it here, since it appears naturally in the analysis presented in Sections IV and V. The beam coverage is related to the beam width of the antenna. As an example, the beam coverage of a rectangular beam is the product of the beamwidths in azimuth and elevation. It should be noticed that the beam coverage solid angle differs from the related term "beam solid angle" [32], [33] which is more commonly encountered. The two terms are equal for antenna gains which are constant within the footprint of the antenna; they otherwise differ. However, for antennas with only small sidelobes, the beam solid angle may be used as an approximation for the beam coverage.

To shorten our notation and terminology, we further define the beam coverage (fraction) as

$$\omega = \frac{|\mathcal{O}|}{4\pi}. \tag{6}$$

The beam coverage fraction ranges from zero to one and can be interpreted as the probability that a wave impinging from a uniformly random direction is within footprint of the antenna. We mention here that $\omega = 1$ for the isotropic antenna, and $\omega = 1/2$ for a hemisphere antenna. Further examples are given in Section VII. We remark that the relation between beam coverage fraction and beamwidth is not one-to-one. Two antennas with the same beamwidth may have different beam coverages and vice versa due to the shape of main-lobes and presence of sidelobes. In fact, is easy to construct examples where such a situation occur; see e.g. the simulation setups in Section VII where both the beam coverage fractions and the beam widths are reported.

III. Mirror Sources and Multipath Parameters

For the defined setup, mirror source theory predicts that the received signal is an infinite sum of attenuated, phase-shifted and delayed signal components as in (1). Unlike Turin's model, in this case the pairs of delay and complex amplitudes $\{(\tau_k, \alpha_k)\}$ do not form a marked Poisson process but are given by the geometry of the propagation environment. The complex gains and delays are readily described using the theory of mirror sources as follows.

To construct the path from transmitter T to receiver R via a single reflection at wall W we determine the position of mirror source T' by mirroring T in W. Thereby, the interaction point can be determined as the wall's intersection with the straight line segment from T' to R. The two-bounce path $T - W_{x-} - W_{x+} - R$ may be constructed by mirroring wall W_{x-} in wall W_{x+} to construct W'_{x-} and then mirroring T' in W'_{x-}. Repeating this procedure *ad infinitum* gives an infinite set of mirror sources and mirror rooms as illustrated in Figure 2.

The position of mirror source k can be computed as

$$r_{T(k_x,k_y,k_z)} = \begin{bmatrix} \left\lceil \frac{k_x}{2} \right\rceil \cdot 2L_x + (-1)^{k_x} \cdot x_T \\ \left\lceil \frac{k_y}{2} \right\rceil \cdot 2L_y + (-1)^{k_y} \cdot y_T \\ \left\lceil \frac{k_z}{2} \right\rceil \cdot 2L_z + (-1)^{k_z} \cdot z_T \end{bmatrix}, \tag{7}$$

where k_x is the number of reflections on the two walls parallel to the yz-plane, i.e. W_{x-} and W_{x+}. Path k interacts with wall W_{x-} in total $\left|\left\lfloor \frac{k_x}{2} \right\rfloor\right|$ times and with wall W_{x+} in total $\left|\left\lceil \frac{k_x}{2} \right\rceil\right|$ times. The indices k_y and k_z are defined analogously. Hence, the path index k corresponds to a triplet $k = (k_x, k_y, k_z)$. Alternatively, the same path can be constructed by introducing a *mirror receiver* at position r_{Rk} determined by replacing subscript T by subscript R in (7). Notice the direct (or line-of-sight) path is also included for $k = (0, 0, 0)$, since for this case $r_{T(0,0,0)} = r_T$ and $r_{R(0,0,0)} = r_R$. For notational brevity, we use subscript $k = 0$ instead of $k = (0, 0, 0)$ for entities related to the direct path throughout the paper.

The signal emitted by mirror source k arrives at the receiver with delay τ_k. Analogously, the signal emitted by the transmitter observed by mirror receiver k has the same delay τ_k. The delay of path k be computed from the positions of mirror source k or mirror receiver k as

$$\tau_k = \|r_{Tk} - r_R\|/c = \|r_{Rk} - r_T\|/c, \tag{8}$$

where c is the speed of light.

The directions of departure and arrival for each path can also be computed. The direction of arrival of the signal from mirror source k is given by the unit vector

$$\Omega_{Rk} = \frac{r_{Tk} - r_R}{\|r_{Tk} - r_R\|}. \tag{9}$$

Similarly, the direction of departure of path k denoted by Ω_{Tk} and can be computed from (9) by interchanging subscripts T and R. It follows that directions of departure and arrival of a specific path are related as

$$\Omega_{Tk} = - \begin{bmatrix} (-1)^{k_y+k_z} & & \\ & (-1)^{k_x+k_z} & \\ & & (-1)^{k_x+k_y} \end{bmatrix} \Omega_{Rk}. \tag{10}$$

In particular, for the direct path $\Omega_{T0} = -\Omega_{R0}$.

Finally, the gain of path k can be specified. We shall not be concerned with the phase of the complex gain α_k, but only its squared magnitude, i.e. the corresponding power gain. The power gain of path k reads

$$|\alpha_k|^2 = g_k \cdot \frac{G_T(\Omega_{Tk}) G_R(\Omega_{Rk})}{(4\pi c \tau_k / l_c)^2}, \tag{11}$$

This article has been accepted for publication in a future issue of this journal, but has not been fully edited. Content may change prior to final publication. Citation information: DOI 10.1109/TAP.2018.2846785, IEEE Transactions on Antennas and Propagation

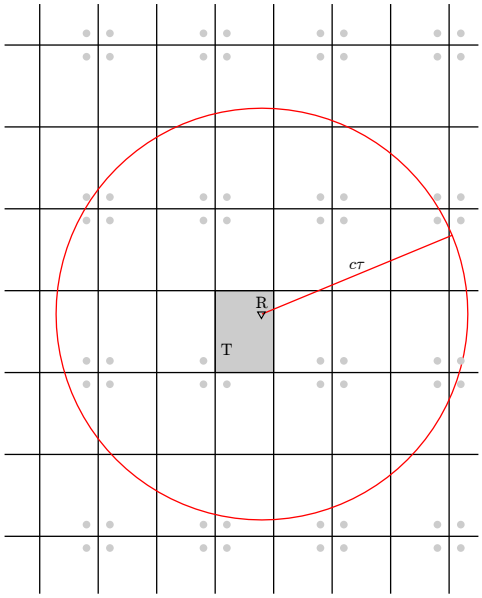

Fig. 2. The rectangular room seen from above with transmitter T and a receiver R and a number of mirror rooms. The pattern continues similarly in the direction perpendicular to the drawing plane. Contributions from mirror sources inside the sphere of radius $c\tau$ arrive at the receiver at delays smaller than τ.

where the factor g_k denotes the gain due to reflections on the walls, the numerator accounts for the transmitter and receiver antennas, and the denominator is due to the attenuation of a spherical wave with l_c denoting the wavelength. Consequently,

$$g_k = g_{x-}^{\left|\lfloor \frac{k_x}{2} \rfloor\right|} g_{x+}^{\left|\lceil \frac{k_x}{2} \rceil\right|} g_{y-}^{\left|\lfloor \frac{k_y}{2} \rfloor\right|} g_{y+}^{\left|\lceil \frac{k_y}{2} \rceil\right|} g_{z-}^{\left|\lfloor \frac{k_z}{2} \rfloor\right|} g_{z+}^{\left|\lceil \frac{k_z}{2} \rceil\right|}. \quad (12)$$

We remark that for the direct path the expression (11) reduces to the Friis equation [34] for propagation in free space.

IV. Analysis of Deterministic Mirror Source Model

The equations (7)–(12) specify the mirror source model well enough for simulations purposes, but are difficult to interpret directly. To better understand the behavior of the model we next consider approximations for the arrival count and rate. In this section the antenna positions and orientations are deterministic. Later, in Section V, we randomize these variables.

A. Arrival Count

The arrival count $N(\tau)$ is defined as the number of paths contributing to the received signal components up to and including a certain time τ. For a path to contribute, the corresponding mirror source should be within a radius $c\tau$ of the receiver, see Fig. 2, and within the footprints of both antennas. Thus the arrival count can be expressed as

$$N(\tau) = \sum_k \mathbb{1}(\tau_k \leq \tau) \cdot \mathbb{1}(\Omega_{Tk} \in \mathcal{O}_T) \cdot \mathbb{1}(\Omega_{Rk} \in \mathcal{O}_R). \quad (13)$$

The exact count depends on the antenna positions, orientations and on the specific antennas. Considering the case with isotropic antennas, the two rightmost indicators are unity and we can approximate the arrival count as the volume of a sphere of radius $c\tau$ divided by the room volume. This argument leads to the cubic approximation for the arrival count proposed by Eyring's approximation [22]:

$$N(\tau) \approx \frac{4\pi c^3 \tau^3}{3V}, \qquad \tau \gg 0. \quad (14)$$

We now develop an approximation for the arrival count by adapting Eyring's analysis to the case with directive antennas and assume a certain fixed line-of-sight delay. Consider first the term due to the direct component, i.e.

$$\mathbb{1}(\tau_0 \leq \tau)\mathbb{1}(\Omega_{T0} \in \Omega_T)\mathbb{1}(\Omega_{R0} \in \Omega_R). \quad (15)$$

Notice that the factor $\mathbb{1}(\Omega_{T0} \in \Omega_T)\mathbb{1}(\Omega_{R0} \in \Omega_R)$ is an indicator of line-of-sight propagation. This factor is unity if line-of-sight propagation occurs, and zero otherwise. Thus if information about the presence of line-of-sight propagation is available, this term is known. If this is not the case, we chose as a compromise to approximate this term as the product $\omega_T \omega_R$. As a shorthand, we introduce the line-of-sight indicator as

$$I_{\text{LOS}} = \begin{cases} 1, & \text{line-sight-sight state,} \\ 0, & \text{non-line-sight-sight state,} \\ \omega_T \omega_R, & \text{unknown state.} \end{cases} \quad (16)$$

Secondly, the number of mirror sources with delay less than τ equals the number of mirror sources inside the sphere with radius $c\tau$ centered at the receiver. For $c\tau$ large compared to the diagonal of the room, i.e. $c\tau \gg \sqrt{L_x^2 + L_y^2 + L_z^2}$, the number of such mirror sources is approximately

$$\frac{4\pi c^3(\tau^3 - \tau_0^3)}{3V}, \quad (17)$$

where we include one mirror source per room volume and subtract the contribution due to the volume closer than $c\tau_0$ to the receiver. Thirdly, only a fraction, ω_R, of these mirror sources are picked up by the receiver. Ignoring the dependency between the direction of departure and arrival for indirect components, we account for the transmit antenna by a factor ω_T. By this line of reasoning

$$N(\tau) \approx \mathbb{1}(\tau \geq \tau_0) \left[I_{\text{LOS}} + \frac{4\pi c^3(\tau^3 - \tau_0^3)\omega_T \omega_R}{3V} \right]. \quad (18)$$

In the special case of isotropic and colocated antennas expression (18) equals Eyring's approximation (14) plus a one due to the line-of-sight component.

B. Arrival Rate

The arrival rate, denoted by $\lambda(\tau)$, is expected number of signal components arriving at the receiver per unit time at delay τ which can be defined in terms of the arrival count such that the expression

$$\mathbb{E}[N(\tau)] = \int_0^\tau \lambda(t) dt \quad (19)$$

This article has been accepted for publication in a future issue of this journal, but has not been fully edited. Content may change prior to final publication. Citation information: DOI 10.1109/TAP.2018.2846785, IEEE Transactions on Antennas and Propagation

holds true. Essentially, $\lambda(\tau)$ can be thought of as a "derivative" of $\mathbb{E}[N(\tau)]$ with respect to τ. However, since the count $N(t)$ is deterministic, we see that $\mathbb{E}[N(\tau)]$ equals $N(\tau)$. The count is a step function and therefore $\lambda(\tau)$ should be interpreted in the distribution sense as a Radon-Nikodym derivative (with respect to Lebesque measure) which leads to:

$$\lambda(\tau) = \sum_k \delta(\tau - \tau_k) \cdot \mathbb{1}(\Omega_{Tk} \in \mathcal{O}_T) \cdot \mathbb{1}(\Omega_{Rk} \in \mathcal{O}_R), \quad (20)$$

where $\delta(\,\cdot\,)$ is Dirac's delta function. Again, the exact count yields no valuable interpretation. Instead by inserting the approximation (18) for the arrival count into (19) we approximate the arrival rate as

$$\lambda(\tau) \approx \delta(\tau - \tau_0) I_{\text{LOS}} + \mathbb{1}(\tau > \tau_0) \frac{4\pi c^3 \tau^2}{V} \omega_T \omega_R. \quad (21)$$

The approximation (21) is clearly not valid point-wise, but should be seen as the average number of arrivals per time unit in a small time interval centered at τ.

The expression (21) gives rise to a number of observations. First, the arrival rate is quadratic in delay which is in sharp contrast to the widespread Saleh-Valenzuela model [5] where the delays of each "cluster" of components has constant arrival rate. [2] Moreover, considering that clusters also arrive at constant rate, the overall arrival rate is only linearly increasing in delay [11]. Secondly, the arrival rate in (21) is inversely proportional to the room volume for $\tau > \tau_0$. Thus, larger rooms lead to smaller arrival rates. This implies that attempts to empirically characterize arrival rates for inroom channels should pay attention to the room size. Finally, we observe that the antennas affect the arrival rate by a delay-independent scaling. Thus very directive antennas lead to a sparser channel in the early part of the channel response, in agreement with experimental results presented in [28]–[31]. However, the arrival rate still grows quadratically and eventually the components in the response merge into a diffuse tail.

V. Analysis of Randomized Mirror Source Model

In the previous section, antenna positions and orientations were held fixed. In the sequel, we let the position and orientation of the transmitter be random. Thus we consider the case where the line-of-sight state is unknown. These assumptions are made here to obtain exact mathematical results and relate thise to the approximation presented Section IV. The considered situation is, however, directly relevant in some applications, e.g. in the initial steps of so-called "beam training algorithms" considered for future millimeter wave systems [36] where the line-of-sight state and direction are yet unknown.

[2] As noted in [35], the constant rate model is justified by several authors as a "convenient compromise" between increasing number of posible multipath components and the increasing shadowing probability. Nevertheless, as also noted in [35], there seems to be no principal reason that the effects should balance each other out to produce exactly a constant rate. Here, we give a clear physical argumentation based mirror source theory for a quadratic rate model.

A. Mean Arrival Count and Arrival Rate

Suppose that the position and orientation of the receiver antenna is fixed. In contrast hereto, the transmitter's position is random with a uniform distribution on the room, i.e. that $r_T \sim \mathcal{U}([0, L_x] \times [0, L_y] \times [0, L_z])$. Furthermore, let the transmitter's orientation be random according to a uniform distribution on the sphere. The counting variable $N(\tau)$ is random with mean

$$\mathbb{E}[N(\tau)] = \mathbb{E}\big[\sum_k \mathbb{1}(\tau_k < \tau) \cdot \mathbb{1}(\Omega_{Tk} \in \mathcal{O}_T) \cdot \mathbb{1}(\Omega_{Rk} \in \mathcal{O}_R)\big]. \quad (22)$$

Since the orientation of the transmitter antenna is uniformly random, the probability for any particular fixed direction, to reside in the random footprint $\mathcal{O}_T$, equals the beam coverage ω_T. Thus, we have the conditional mean,

$$\mathbb{E}[\mathbb{1}(\Omega_{Tk} \in \Omega_T) | \Omega_{Tk}] = \omega_T \quad (23)$$

irrespective of the particular value of Ω_{Tk}. Each mirror source is uniformly distributed within its mirror room, and therefore mirror source positions constitue a homogeneous (but not Poissonian) random spatial point process with intensity $1/V$. Then, inserting (23) and using Campbell's theorem [37], we can rewrite the expectation as an integral over mirror source positions

$$\begin{aligned}\mathbb{E}[N(\tau)] &= \frac{\omega_T}{V} \int \mathbb{1}\left(\tfrac{\|r - r_R\|}{c} < \tau\right) \mathbb{1}\left(\tfrac{r - r_R}{\|r - r_R\|} \in \mathcal{O}_R\right) dr \\ &= \frac{4\pi c^3 \tau^3}{3V} \omega_T \omega_R \mathbb{1}(\tau > 0). \end{aligned} \quad (24)$$

Taking the derivative of the expected arrival count, we obtain the corresponding arrival rate

$$\lambda(\tau) = \frac{4\pi c^3 \tau^2}{V} \omega_T \omega_R \mathbb{1}(\tau > 0). \quad (25)$$

It follows by simple modifications of the above argument that the same results hold true for a number of different cases:

1) Transmitter with fixed orientation and uniform position; receiver with uniform orientation and fixed location.
2) Either of the antennas are isotropic and either of the antenna locations are uniform.
3) Transmitter position and orientation are uniform and independent of the receiver position and orientation.
4) Transmitter position and antenna orientation are uniform conditioned on the receiver position and orientation.

Obviously, Case 4) implies Cases 1) through 3). Moreover, by symmetry, any of the above results hold true if the transmitter and receiver swap roles.

This quadratically increasing rate bears witness of the gradual transition in the impulse response that consists of separate specular components at early delays to a late diffuse tail consisting of myriads of specular components. We remark that for isotropic antennas Eyring's approximation (see (14)) is equal to our expression for the mean count. In this sense, Eyring's approximation is not only valid asymptotically, but is exact in the mean. The inclusion of the beam coverages is a natural extension to the non-isotropic case.

The relative ease by which we derived the mean arrival count (24) may lead us to think that perhaps also higher

This article has been accepted for publication in a future issue of this journal, but has not been fully edited. Content may change prior to final publication. Citation information: DOI 10.1109/TAP.2018.2846785, IEEE Transactions on Antennas and Propagation

moments could be easily derived. However, it proves much more challenging to derive its second moment—in fact we have not been able to establish an exact expression. We give an approximation in Appendix A. Similarly, it is difficult to get exact formulas if less randomness is introduced in the model. To that end, Appendix B gives an upper bound to the mean arrival rate for the case where the transmitter antenna has random position, but fixed orientation; Appendix C gives an approximation for the mean count for fixed transmitter-receiver distance known/unknown line-of-sight state.

B. Mixing Time

Commonly we consider a channel impulse response consisting of so many specular components that each of these cannot be separated by the receiver as "diffuse". It is well known that in the inroom scenario, a specular-to-diffuse transition from early separate components to a later diffuse tail can be observed. Impulse response models that includes both specular and diffuse components must account for this transition in some way. In the literature this has been done in various ways, see e.g. [9], [19], [26], [38]–[40]. The model studied here also leads to a specular-to-diffuse transition. The simple quadratic expression for the arrival rate (25) enable us to give a definition of the onset of the diffuse tail by analogy to room acoustics.

In the room acoustics literature, a similar diffusion process have been studied intensively for over a century [41]. A useful and widespread characteristic of the diffuse tail's onset is the so-called "mixing time". In [42], the mixing time defined as the delay at which a listener is no longer able to distinguish individual echoes. In analogy thereto, we propose to define mixing time τ_{mix} for room electromagnetics. The mixing time should indicate the delay value beyond which the receiver can no longer be expected to distinguish the signal components of individual paths. If the receiver in a system with signal bandwidth B can distinguish on average up to N_{mix} signal components per pulse duration, we can find the mixing time by solving the equation

$$N_{\mathrm{mix}} = \int_{\tau_{\mathrm{mix}}-\frac{1}{2B}}^{\tau_{\mathrm{mix}}+\frac{1}{2B}} \lambda(\tau) d\tau. \tag{26}$$

Inserting (25) and solving for τ_{mix} gives the expression

$$\tau_{\mathrm{mix}} = \sqrt{\frac{N_{\mathrm{mix}} BV}{4\pi c^3 \omega_T \omega_R} - \frac{1}{12B^2}}, \tag{27}$$

where $\tau_{\mathrm{mix}} > 1/2B$ was assumed.

Fig. 3 shows the mixing time versus $B/\omega_T\omega_R$ for a range of room volumes. The number N_{mix} of components that can be distinguished within a pulse duration depends on the particular system in question. Determining this value is beyond the scope of the present investigation and thus we set it to unity in Fig. 3.

For large signal bandwidth, the mixing time attains the asymptote

$$\tau_{\mathrm{mix}} = \sqrt{N_{\mathrm{mix}}} \sqrt{\frac{BV}{4\pi c^3 \omega_T \omega_R}}. \tag{28}$$

Thus to determine the large bandwidth asymptote of the mixing time for N_{mix} different from unity is obtained by a scaling by $\sqrt{N_{\mathrm{mix}}}$. In the large bandwidth case, the mixing time is proportional to the square root of the room volume which is quite intuitive: larger rooms have longer mixing times. Moreover, the mixing time is inversely proportional to the square root of the beam coverages: more directive antennas lead to a later onset for the diffuse tail. Finally, by increasing the system bandwidth, the mixing time increases by the square root of the bandwidth. The mixing time determines if a diffuse reverberation tail can be observed in noise limited measurements. The diffuse tail appears only if the power-delay spectrum exceeds the noise floor at the mixing time, and is otherwise masked by noise.

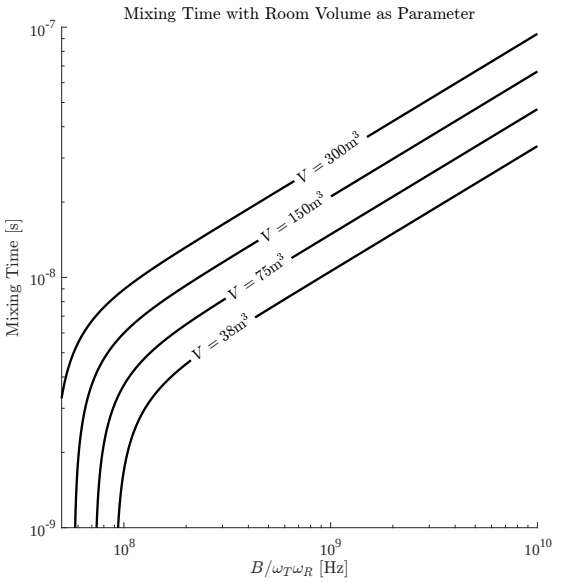

Fig. 3. Mixing time versus $B/\omega_T\omega_R$ for different room volumes with $N_{\mathrm{mix}} = 1$.

VI. Approximation for Power-Delay Spectrum

We now turn to the question of approximating the power-delay spectrum. As in Section V, we consider the case where the position and orientation of the transmitter is random and the line-of-sight state is unknown. The case of deterministic transmitter-receiver distance and known line-of-sight state is discussed in Appendix C.

As can be seen from the product form in (3), the power delay spectrum is factorized into the arrival rate and the conditional second moment $\sigma_\alpha^2(\tau)$ of the complex gain. We already derived the arrival rate in (25), so it only remains to derive an (approximate) expression for $\sigma_\alpha^2(\tau)$. To this end, we follow an adaptation of Eyring's approach [22].

Let the average wall gain be defined as

$$\bar{g} = \frac{1}{S}\sum_i S_i g_i, \tag{29}$$

where wall i has area S_i and gain g_i, and the total surface area of the room is

$$S = \sum_i S_i = 2(L_xL_y + L_xL_z + L_yL_z). \tag{30}$$

This article has been accepted for publication in a future issue of this journal, but has not been fully edited. Content may change prior to final publication. Citation information: DOI 10.1109/TAP.2018.2846785, IEEE Transactions on Antennas and Propagation

Here, the second equality is due to the rectangular room geometry. Replacing the individual wall gains in (12) by the average value $\bar{g}$, we approximate the gain of path k as

$$|\alpha_k|^2 \approx \bar{g}^{|k|} \cdot \frac{G_T(\Omega_{Tk})G_R(\Omega_{Rk})}{(4\pi c\tau_k/l_c)^2}, \tag{31}$$

with the convention $|k| = |k_x| + |k_y| + |k_z|$ for the number of wall interactions of path k.

For a given path length $c\tau_k$, the number of interactions $|k|$ varies according to the positions of the transmitter and receiver and the orientation of the path. As Eyring further noted in [22], the number of wall interactions for mirror source k can be approximated as the path length $c\tau_k$ divided by the mean chord length of a room which is $4V/S$ [22], [41], [43]. Hence, we insert

$$|k| \approx \tau_k \cdot \frac{cS}{4V} \tag{32}$$

into (11) to obtain

$$|\alpha_k|^2 \approx \begin{cases} \bar{g}^{\tau_k cS/4V} \cdot \frac{G_T(\Omega_{Tk})G_R(\Omega_{Rk})}{(4\pi c\tau_k/l_c)^2}, & k \neq (0,0,0) \\ \frac{G_T(\Omega_{T0})G_R(\Omega_{R0})}{(4\pi c\tau_0/l_c)^2}, & k = (0,0,0). \end{cases} \tag{33}$$

The factor $g^{\tau_0 cS/4V}$ is close to unity if τ_0 is small compared to the mean chord length of the room, or if $\bar{g}$ is close to unity. In this case,

$$\mathbb{E}[|\alpha_k|^2|\tau_k] \approx \frac{\bar{g}^{\tau_k cS/4V}}{(4\pi c\tau_k/l_c)^2} \cdot \mathbb{E}\left[G_T(\Omega_{Tk})G_R(\Omega_{Rk})\middle|\tau_k\right], \tag{34}$$

where the expectation at the right-hand side is with respect to the directions of arrival and the orientation of the transmitter antenna.

This expectation can be computed by first invoking the law of total expectation:

$$\mathbb{E}\left[G_T(\Omega_{Tk})G_R(\Omega_{Rk})\middle|\tau_k\right] = \mathbb{E}\left[\mathbb{E}\left[G_T(\Omega_{Tk})\middle|\Omega_{Rk},\tau_k\right] G_R(\Omega_{Rk})\middle|\tau_k\right]. \tag{35}$$

Due to the one-to-one relation (10) between the arrival and departure direction, it is clear that for a given direction of arrival, the direction of departure is also fixed. Therefore the innermost expectation in (35) is the expected gain of a uniformly oriented antenna evaluated in a fixed direction within its footprint:

$$E\left[G_T(\Omega_{Tk})\middle|\Omega_{Rk},\tau_k\right] = \frac{1}{|\mathcal{O}_T|}\int_{\mathcal{O}_T} G_T(\Omega)d\Omega = \frac{1}{|\mathcal{O}_T|}\int_{\mathbb{S}_2} G_T(\Omega)d\Omega = \frac{1}{\omega_T}. \tag{36}$$

It now remains to compute the expectation $\mathbb{E}\left[G_R(\Omega_{Rk})\middle|\tau_k\right]$. The mirror source process homogeneous and therefore the direction of paths impinging on the receive antenna is uniformly distributed on the sphere. Therefore, the direction of arrival (of a path actually received by the antenna) is uniformly distributed within the footprint, hence

$$\mathbb{E}\left[G_R(\Omega_{Rk})\middle|\tau_k\right] = \frac{1}{|\mathcal{O}_R|}\int_{\mathbb{S}_2} G_R(\Omega)d\Omega = \frac{1}{\omega_R}. \tag{37}$$

Finally, inserting (35),(36), and (37) into (34) yields

$$\sigma_\alpha^2(\tau) \approx \frac{\bar{g}^{\tau cS/4V}}{(4\pi c\tau/l_c)^2} \cdot \frac{1}{\omega_T\omega_R}. \tag{38}$$

Together the expressions (25), (38) and (3) gives an approximation for the power-delay spectrum:

$$P(\tau) \approx \mathbb{1}(\tau > 0)\frac{e^{-\tau/T}}{4\pi V/l_c^2 c}, \tag{39}$$

with the reverberation time T defined as

$$T = -\frac{4V}{cS\ln(\bar{g})}. \tag{40}$$

This expression for the reverberation time is the same as obtained in Eyring's model [17], [22].

The power-delay spectrum takes the form of an exponentially decaying function. This is interesting in the light of the super-exponential decay of the per-path gain in (31). However, this super-exponential trend is balanced out by the quadratic increase in arrival rate such that the net result is an exponential decay.

It is a remarkable and perhaps surprising fact that the approximate power-delay spectrum in (39) is unaffected by the directivity of the antenna. Indeed, the antennas enter in both the arrival rate and in the conditional gain, but these effects cancel in the power-delay spectrum. Thus neither the total expected power nor the reverberation time change with antenna directivity. Obviously, the individual realizations of the received signal are vary greatly with the particular antenna responses, positions and orientations. However, this dependency vanishes when taking the expectation over all transmitter positions and orientations.

The aspect ratio of the room enter in the expression (39) only via the ratio V/S in (40). In fact some information of the aspect ration is lost due to the approximation in (32). The accuracy of (32) can be improved by incorporating more complex models such as the ones developed for room acoustics, see [41], [44]. As an example, the modification introduced in [41] improves the approximation in (32) by adjusting the reverberation time by a correction factor ξ defined as

$$\xi = \frac{1}{1 + \gamma^2\ln(\bar{g})/2}. \tag{41}$$

The constant γ^2, which depends on the aspect ratio of the room, can be determined by Monte Carlo simulation and typically takes values in the range 0.3 to 0.4 [41]. The particularities of such corrections are of less importance here, and therefore further refinements of (41) are left as future work.

VII. Numerical Examples

We now illustrate the derived theoretical results by comparing the theoretical results to simulations of the mirror source model in a particular setup.

This article has been accepted for publication in a future issue of this journal, but has not been fully edited. Content may change prior to final publication. Citation information: DOI 10.1109/TAP.2018.2846785, IEEE Transactions on Antennas and Propagation

A. Simulation Method

The equations (7)–(12) allow for simulating the received signal in a straight forward manner. First a set of mirror sources positions are constructed using (7) with the associated multipath parameters obtained by evaluating (8)–(12). Since the set of mirror sources is clearly infinite, a stopping criterion is required to ensure finite computational complexity. Here we chose to simulate all mirror sources with a delay up to a predefined time $\tau_{\max}$. The received signal can be obtained by (1) for a specified transmitted signal. Based on the multipath parameters, the arrival count (13) is evaluated by first removing paths that with direction of arrival or departure outside the antenna footprints. Then the arrival count can be computed by computing the unnormalized empirical distribution function (ecdf) for which ready-made routines exists in most scientific programming packages. The arrival rate can be estimated using a kernel-density estimate, which is also widely available.

In the deterministic case, the model is evaluated for particular antenna positions and orientations. The randomized model is evaluated by simulating a large number of independent Monte Carlo runs. In each run, one position of the transmit antenna position and orientation is generated uniformly by draws from pseudo-random number generators.

B. Simulation Setup

Table I specifies the simulation settings. In the numerical examples we consider for simplicity the same gain value g for all walls. The transmitted signal $s(t)$ is a sinc pulse with constant Fourier transform over the considered frequency band, and zero elsewhere.

We consider in our simulations two different types of idealized antennas both defined with the beam coverage as a parameter (setting $\epsilon = 0$). The first type is an idealized sector antenna with constant gain over the spherical cap centered at the direction given by the unit vector ζ:

$$G_{\text{sector}}(\Omega) = \frac{1}{\omega}\mathbb{1}(\Omega^T\zeta \geq 1 - 2\omega). \tag{42}$$

This antenna gain exhibits neither back- nor side-lobes. For the sector antenna, the half-beamwidth is $\arccos(1-2\omega)$ and gain $1/\omega$ over an isotropic antenna. For the special case of $\omega = 1$ the isotropic pattern is obtained; $\omega = 1/2$ gives the hemisphere antenna. Arbitrarily narrow beams can be obtained by setting ω to sufficiently small values. The second antenna type is a sector antenna with front- and back-lobes:

$$G_{\text{backlobe}}(\Omega) = \frac{4}{3\omega}\mathbb{1}(\Omega^T\zeta \geq 1 - \omega) + \frac{2}{3\omega}\mathbb{1}(\Omega^T\zeta \leq \omega - 1). \tag{43}$$

This antenna has a half-beamwidth $\arccos(1-\omega)$ and the the front-to-back ratio is 3 dB.

In the simulations we consider different settings of the beam coverages as given in Table II. For ease of comparison we also report in the table, the resulting half-beamwidth and gain. It is clear from the table that the beam coverage does not map one-to-one to the half-beamwidth. We remark that we for simplicity reason simulate only antenna responses that are rotationally symmetric about the direction ζ. Furthermore, in all cases considered, the transmitter and receivier are equipped with identical antennas. These choices are made for simplicity of the simulation, and is not a limitation of the derived theory.

TABLE I
SIMULATION SETTINGS

Room dim., $L_x \times L_y \times L_z$	$5 \times 5 \times 3\,\text{m}^3$
Reflection gain, g	0.6
Center Frequency	60 GHz
Bandwidth, B	2 GHz
Speed of light, c	$3 \cdot 10^8\,\text{m/s}$
Maximum delay, $\tau_{\max}$	120 ns
Transmitted signal, $s(t)$	Sinc pulse
No. Monte Carlo Runs	10 000

TABLE II
ANTENNA SETTINGS

Antenna Type	ω	Half-beamwidth	Gain [dBi]
Sector (Isotropic)	1	180°	0
Sector (Hemisphere)	0.5	90°	3
Sector	0.25	60°	6
Backlobe	1	90°	3
Backlobe	0.5	60°	6
Backlobe	0.25	41.1°	9

C. Deterministic Case

We consider first the example with the orientation and positions of the antennas are deterministic. In this example, we orient the antennas in direction of line-of sight, i.e. $\zeta_T = \Omega_{T0}$ and $\zeta_R = \Omega_{R0}$. Then direct propagation occurs and $I_{\text{LOS}} = 1$. Figs. 4 and 5 show received signals and arrival counts for sector and backlobe antennas given in Table II.

The general trend is that the received signal decays exponentially with delay while the signal contributions gradually merge into a diffuse tail. As can be seen, the rate of diffusion depends on the antenna: smaller beam coverage leads to a slower diffusion process with a sparser response in which each signal component having higher gain. This effect accord with the mixing times also indicated in the plots. Moreover, for the same beam coverage setting, the received signals are similar for the sector and backlobe antennas. The corresponding arrival counts is observed to fluctuate about their respective approximation given by (18). The count clearly depends on the particular antenna type, but approach the same approximation for different antennas with equal beam coverages.

The fluctuations of the count about the approximation appear to be larger at smaller counts, which can be primarily attributed to the double logarithmic scale which magnify visually the errors at small counts, while deemphasising errors at large counts. Furthermore, the approximation is essentially to approximate the number of mirror sources inside a section of a sphere by the number of mirror source volumes within that sector. This approximation is more accurate if the sphere is large compared to the room size, which is the case at large delays.

D. Randomized Model

We now compare the theoretical results derived for the randomized model with Monte Carlo simulations. The sim-

This article has been accepted for publication in a future issue of this journal, but has not been fully edited. Content may change prior to final publication. Citation information: DOI 10.1109/TAP.2018.2846785, IEEE Transactions on Antennas and Propagation

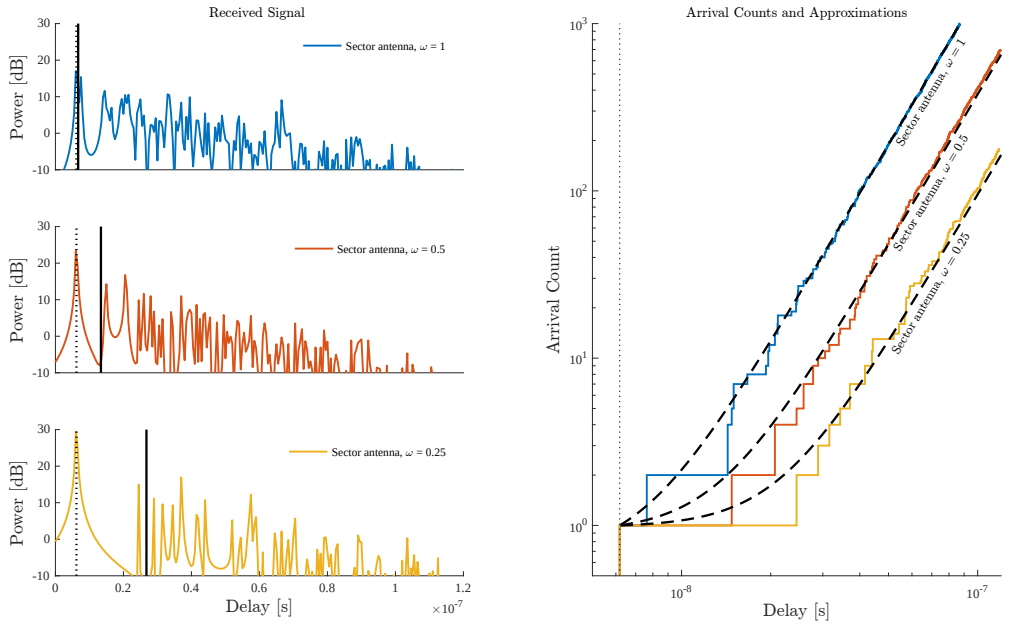

Fig. 4. Magnitude squared received signal and arrival counts for the three different sector antennas in Table II. Line-of-sight delay is indicated by a vertical dotted line and mixing time is indicated by a vertical solid line. Theoretical approximate counts are shown in black dashed lines. The antennas are located at $r_T = [2.5, 2.5, 1.5]^T$m and $r_R = [1.5, 1.5, 2.7]^T$m and are oriented exactly in direction of line-of-sight. The remaining settings are given in Table I.

ulation settings are listed in Table I. In each Monte Carlo run, the transmitter and receiver antennas are placed uniformly at random within the room and the orientations picked uniformly at random. Thus we simulate a setup for which (24) and (25) apply.

Fig. 6(a) reports arrival counts for different antenna settings along with their respective theoretical mean counts. For each setting of the beam coverage, ten individual arrival counts are shown to exemplify the variations among the realizations. The realizations fluctuate about their respective theoretical mean. We observe that this variation is more pronounced for more directive antennas and at low delays. In Fig. 6(b) the mean count estimated as the average of the arrival counts from all Monte Carlo runs is compared to the theoretical mean count in (24). As expected, the corresponding curves fit almost perfectly. Similarly, the estimated arrival rates matches closely the theoretical values as seen in Fig. 6(c).

Finally, Fig. 6(d) shows the expected power of the received signal, i.e. $\mathbb{E}[|y(t)|^2]$ obtained from the Monte Carlo simulation. We observe that as predicted, the curves for the different antenna settings are identical modulo uncertainties due to the Monte Carlo simulation technique. This observation confirms the observation made in the introduction that models with very different arrival rates, e.g. due to differences in antenna directivity, can indeed lead to the same power-delay spectrum. The simulation is compared with the approximation obtained by using (2) and (39). From Fig. 6(d) it appears that the slope of the theoretical curve, i.e. the reverberation time computed in (40), deviates from the simulation by about 9 %. The fit can be improved by applying the correction factor (41). According to [41], the value $\gamma^2 = 0.30$ can be used for the aspect ratio of the room considered. For our simulation setup, this yields a correction factor of $\xi \approx 1.083$ which gives an excellent fit.

A comparison of Figs. 6 and 7 reveals that the sector and backlobe antennas yield very similar behaviors in terms of mean arrival count, arrival rate and power delay spectrum. The major difference is in fluctuations of individual realizations about the mean arrival count. The backlobe antenna yields more pronounced variation in the arrival count than the sector antenna.

The instantaneous mean delay and rms delay spread are often considered as important parameters for design of radio systems. Theoretical analysis of these entities is beyond the scope of this contribution, but we report some simulated empirical cumulative distribution functions in Figs. 8 and 9. In these simulations the mean delay and rms delay spread are computed as respectively the first and centered second moments of the realizations of $|y(t)|^2$ (thus including the effect of the transmitted pulse). Even though the directional antenna gain pattern does not affect the power delay spectrum, it is apparent from Figs. 8 and 9 that the instantaneous mean delay and rms delay spread vary significantly with the beam coverage.

VIII. Discussion

Some of the predictions of the mirror source analysis can be compared to observations from measurements reported in the open literature. The model for the power delay spectrum has already been validated with measurements in [17]. The validation concerned the relation to room volume, average gain, and surface area. It was found that Eyring's model more accurately predicts the reverberation time than Sabine's model considered more widely in the room electromagnetics literature [12]–[17]. However, due to the typically lower value for $\bar{g}$ observed in room electromagnetics, (approximately 0.6 in [17]), the Sabine model is inaccurate. Moreover, [17, Fig. 5], reports

This article has been accepted for publication in a future issue of this journal, but has not been fully edited. Content may change prior to final publication. Citation information: DOI 10.1109/TAP.2018.2846785, IEEE Transactions on Antennas and Propagation

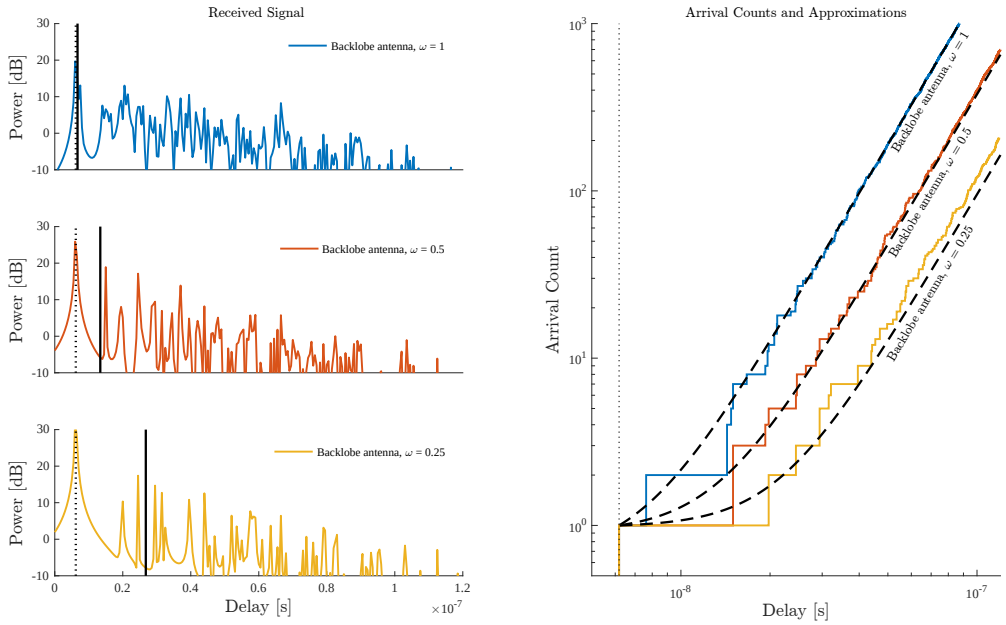

Fig. 5. Magnitude squared received signal and arrival counts for the same setup as in Fig.4, but with three different backlobe antennas as specified in Table II.

the power delay spectrum for an inroom channel averaged over all measured positions in the room. The average power delay spectrum agrees well with an exponentially decaying model similar to (39) with decay rate given by Eyring's reverberation time. Due to the fact that it was not possible to measure at very short distances, the average power delay spectrum in [17, Fig. 5] exhibit an onset at a delay corresponding to the shortest distance included in the measurements. It should be noted here that the validation in [17] is done with respect to the power delay spectrum, received power, and rms delay spread but the arrival rate was not measured. In this scenario however, it turns out to be difficult to distinguish individual multipath components in the received signal.[3]

Predictions of the arrival rate model can be compared qualitatively to previously published measurements. The quadratically increasing arrival gives in combination with a finite bandwidth signal rise to a specular-to-diffuse transition. This transition is routinely observed in inroom scenarios with sufficient measurement bandwidth, see e.g [9], [12], [23], [28]. The effect of directive antennas on the arrival rate appears to be under-explored experimentally. The effect can, however, be observed qualitatively in a few publications e.g. in the early work by Manabe [28] where received signals for an inroom scenario are reported for different antenna configurations. It appears that the received signal becomes sparser in applying more directive antennas. We observe from our simulations reported in Figs. 8 and 9 that for more directive antennas, the rms delay spread reduces. This trend is confirmed by several measurements reported in the literature, see e.g. [28], [31], [45], [46].

To validate the quantitative predictions of the proposed arrival rate model, the dependency on antenna responses and room volume should be checked. Such a validation is currently pending due to the lack of appropriate estimators for the arrival rate. The estimators applied in literature to estimate arrival rate follow a two-step procedure (similar to the method used by Turin [2]): First delays of multipath components are estimated using high-resolution estimators, (e.g. CLEAN [47], ESPRIT [48], SAGE [49], RiMax [50]); then the arrival rate is estimated from the obtained delays. Unfortunately, the delay estimates are inaccurate if applied to channel responses with very high arrival rates, such as the proposed model predicts. As a consequence, this approach may lead to biased estimates of the arrival rate. We remark that to properly validate the model, new estimators for arrival rate should be proposed. We leave the development of such new estimators and thus the quantitative validation as future work.

The presented arrival rate model is based on mirror source analysis applied to an idealized propagation environment, namely an empty rectangular room with flat walls. We note that the diffusion effect is predicted to happen even with an empty room and plane walls. While relevant from a theoretical perspective, this scenario cannot be expected to occur in practical situations. For more complicated scenarios, e.g. in furnished rooms, we conjecture that the arrival rate will increase faster than quadratic. Thus the predicted mixing time may be considered an upper bound for the mixing time in real situations. In such situation, we may consider a more general model for the arrival rate, e.g. the two parameter model

$$\lambda(\tau) = \omega_T \omega_R q \tau^p \mathbb{1}(\tau > 0) \tag{44}$$

where the parameters q and p should be determined. Note that this model generalizes both the arrival rate model in (25) and

[3] In [17] the measurement in bandwidth, $B = 120\,\mathrm{MHz}$, the antennas are omnidirectional hemisphere antennas, $\omega \approx 1/2$ and room volume is $V = 65\,\mathrm{m}^3$. With $N_{\mathrm{mix}} = 1$ this gives the mixing time of 9.6 ns calculated by (28) or slightly lower value 9.3 ns from (27). In this case, the mixing time corresponds to approximately the sampling time and therefore we can expect the multipath components to overlap even the direct component.

This article has been accepted for publication in a future issue of this journal, but has not been fully edited. Content may change prior to final publication. Citation information: DOI 10.1109/TAP.2018.2846785, IEEE Transactions on Antennas and Propagation

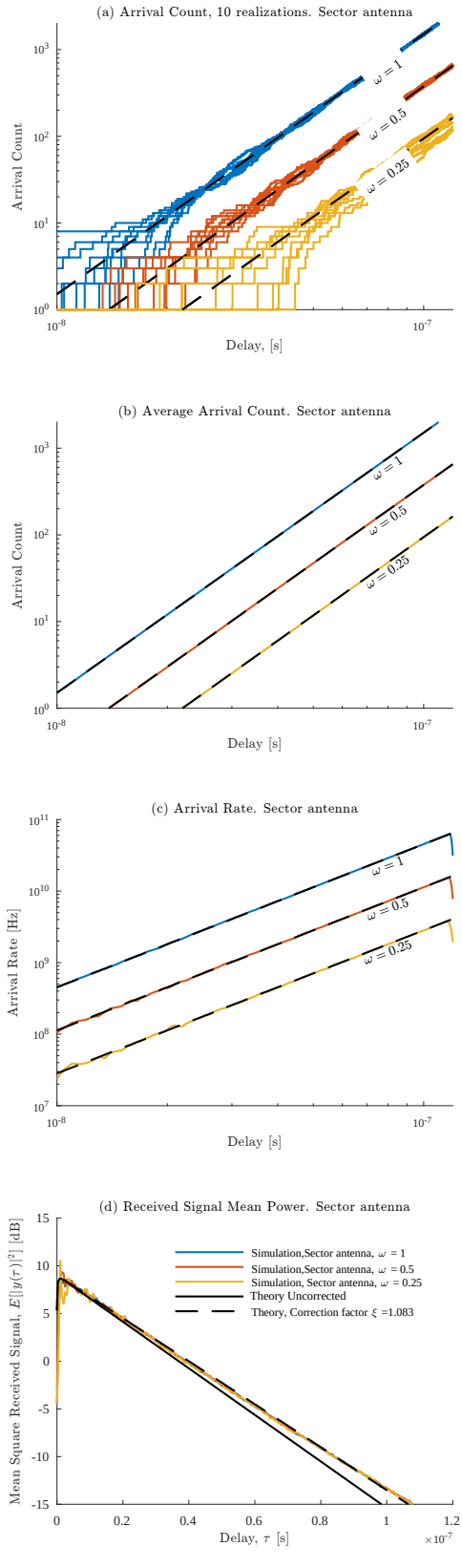

Fig. 6. Simulations (colored lines) and theory (black lines) for randomly placed and oriented sector antennas (a) Realizations of arrival count and theoretical mean count; (b) Mean arrival count; (c) Arrival rate (theory and kernel-density estimate); (d) Mean square received signal. The settings are given in Tables II and I.

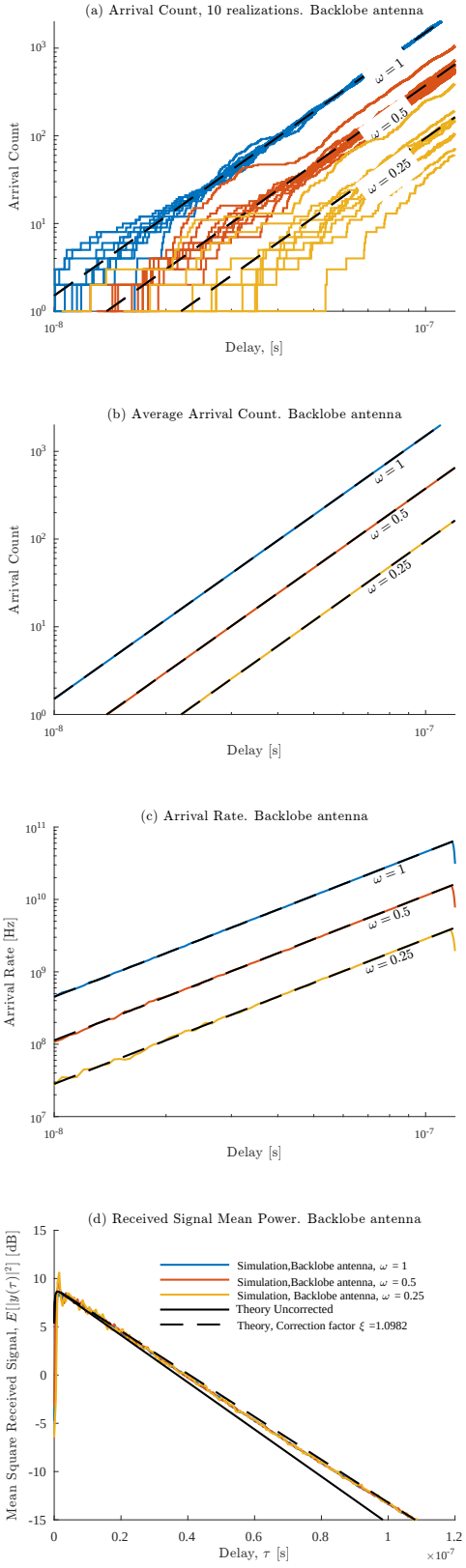

Fig. 7. Simulations (colored lines) and theory (black lines) for the same setup as in Fig. 6, but with backlobe antennas.

This article has been accepted for publication in a future issue of this journal, but has not been fully edited. Content may change prior to final publication. Citation information: DOI 10.1109/TAP.2018.2846785, IEEE Transactions on Antennas and Propagation

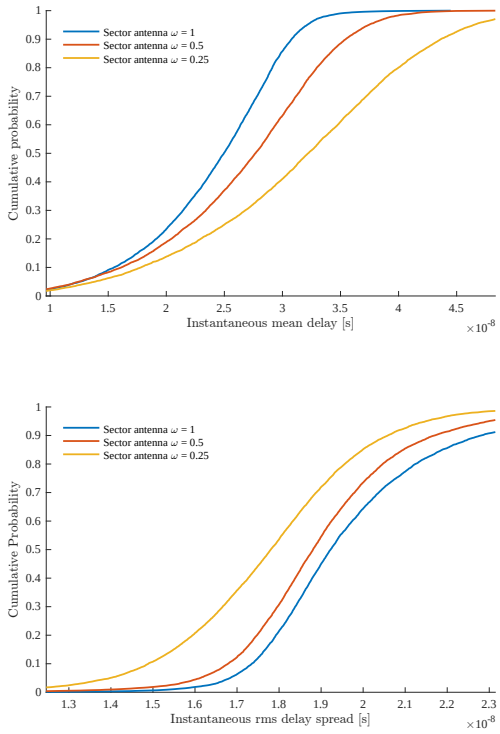

Fig. 8. Empirical cumulative probability of instantaneous mean delay (upper panel) and rms delay spread (lower panel) for the sector antenna. The settings are given in Tables II and I.

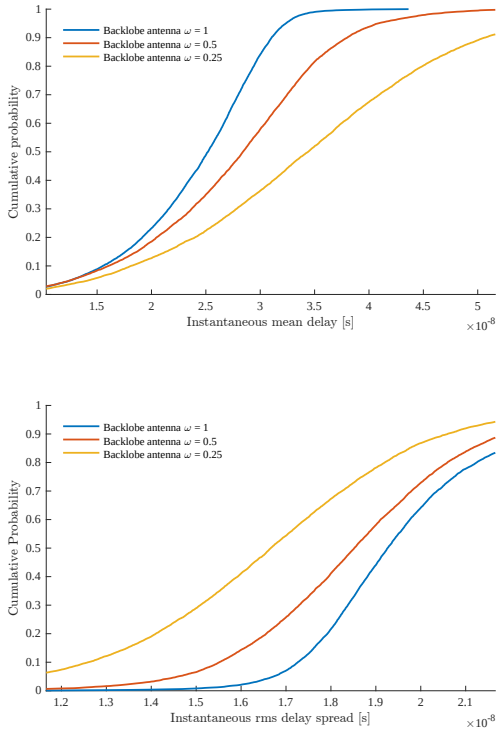

Fig. 9. Empirical cumulative probability of instantaneous mean delay (upper panel) and rms delay spread (lower panel) for the backlobe antenna. The settings are given in Tables II and I.

"constant rate model" at the cost of introducing introducing a second parameter.

IX. Conclusion

The present study shows how the path arrival rate can be analyzed based on mirror source theory for rectangular room which accounts for the antenna directivity. We give an exact formula for the mean arrival count and consequently for the arrival rate for the case where the position and orientation of the transmitter are uniformly random. The rate grows quadratically with delay giving rise to a transition from early isolated signal components gradually merging into a diffuse reverberation tail at later delays. The rate is inversely proportional to the room volume, and thus larger rooms lead to a slower transition. Moreover, the rate is proportional to the product of beam coverage fractions of the transmitter and receiver antennas, and thus more directive antennas yield lower arrival rate. The derived expression quantifies the impact of directive antennas on the arrival rate, a phenomenon observed qualitatively in a number of previous experimental and simulation studies in the literature. The expression for the arrival rate yields a simple formula for the "mixing time", i.e. the point in time at which the mean arrival rate exceeds one component per transmit pulse duration. The mixing time quantifies to what extent non-overlapping signal components is to be expected for a given scenario. The arrival rate expresion can be used to approximate the power delay spectrum which appears to be unaffected by the antenna radiation pattern. However, the antennas do indeed play an important role for other characteristics as exemplified by simulations of the distribution of instantaneous mean delay and rms delay spread.

Acknowledgements

The author thanks Carles Navarro Manchon, Ramoni Adeogun, Gilberto Berardinelli, and Bernard H. Fleury for comments and discussions which helped to improve this work.

Appendix A
Second Moment of Arrival Count

The raw second moment of the arrival count reads

$$\mathbb{E}[N(\tau)^2] = \sum_{k,k'} \mathbb{E}[N_k N_{k'}], \tag{45}$$

with the shorthand notation

$$N_k = \mathbb{1}(\tau < \tau_k)\mathbb{1}(\Omega_{Tk'} \in \mathcal{O}_T)\mathbb{1}(\Omega_{Rk'} \in \mathcal{O}_R)]. \tag{46}$$

Noting that $N_k^2 = N_k$, we see that the sum of diagonal terms ($k = k'$) equals the mean $\mathbb{E}[N(\tau)]$ and thus

$$\mathbb{E}[N(\tau)^2] = \mathbb{E}[N(\tau)] + \sum_{k \neq k'} \mathbb{E}[N_k N_{k'}]. \tag{47}$$

The cross terms ($k \neq k'$), cannot be readily computed. Instead, we approximate the cross terms by considering the positions of the mirror to be uncorrelated:

$$\mathbb{E}[N(\tau)^2] \approx \mathbb{E}[N(\tau)] + \sum_{k,k'} \mathbb{E}[N_k]\mathbb{E}[N_{k'}] \tag{48}$$

$$= \mathbb{E}[N(\tau)]^2 + \sum_{k} (\mathbb{E}[N_k] - \mathbb{E}[N_k]^2). \tag{49}$$

This article has been accepted for publication in a future issue of this journal, but has not been fully edited. Content may change prior to final publication. Citation information: DOI 10.1109/TAP.2018.2846785, IEEE Transactions on Antennas and Propagation

The terms in the last sum are variances of N_k of which most vanish. Only mirror rooms which can be intersected by a sphere of radius $c\tau$ centered at the receiver contribute to this sum. Considering a receiver at the center of the room, for these mirror rooms,

$$\tau - D/2c < \tau_k < \tau + D/2c, \tag{50}$$

where $D = \sqrt{L_x^2 + L_y^2 + L_z^2}$ is the length of the main diagonal of the room. The number of such mirror rooms can be approximated as

$$\mathbb{E}[N(\tau + D/(2c))] - \mathbb{E}[N(\tau - D/(2c))]. \tag{51}$$

Finally, approximating the values of the variances by the maximal variance of a Bernoulli variable, we have

$$\begin{aligned}\mathbb{E}[N(\tau)^2] \approx & \mathbb{E}[N(\tau)]^2 \\ & + \frac{1}{4}(\mathbb{E}[N(\tau + \frac{D}{2c})] - \mathbb{E}[N(\tau - \frac{D}{2c})]).\end{aligned} \tag{52}$$

Monte Carlo simulations (not reported here) for the setup described in Section VII demonstrate that the approximation is reasonably accurate for the raw moment, but overshoots the variance significantly.

Appendix B
Transmitter with Random Position and Fixed Orientation

Let the transmitter's orientation be fixed, but its position be uniformly distributed.The position and orientation of the receiver is fixed. Then the mean arrival count reads

$$\begin{aligned}\mathbb{E}[N(\tau)] &= \mathbb{E}\big[\sum_k \mathbb{1}(\tau_k < \tau) \cdot \mathbb{1}(\Omega_{Tk} \in \mathcal{O}_T) \cdot \mathbb{1}(\Omega_{Rk} \in \mathcal{O}_R)\big] \\ &\leq \mathbb{E}\big[\sum_k \mathbb{1}(\tau_k < \tau) \cdot \mathbb{1}(\Omega_{Rk} \in \mathcal{O}_R)\big],\end{aligned} \tag{53}$$

with equality for isotropic transmitter antenna. By Campbell's theorem,

$$\begin{aligned}\mathbb{E}[N(\tau)] &\leq \frac{1}{V}\int \mathbb{1}\left(\tfrac{\|r - r_R\|}{c} < \tau\right) \mathbb{1}\left(\tfrac{r - r_R}{\|r - r_R\|} \in \mathcal{O}_R\right) dr \\ &= \frac{4\pi c^3 \tau^3}{3V} \cdot \omega_R \mathbb{1}(\tau > 0).\end{aligned} \tag{54}$$

Symmetry gives a similar inequality involving ω_R. In combination, these two lower bound yields

$$\mathbb{E}[N(\tau)] \leq \frac{4\pi c^3 \tau^3}{3V} \cdot \min\{\omega_T, \omega_R\} \mathbb{1}(\tau > 0), \tag{55}$$

again, with equality obtained either of the antennas are isotropic. Since (55) holds for all τ, the arrival rate is upper bounded as

$$\lambda(\tau) \leq \frac{4\pi c^3 \tau^2}{V} \cdot \min\{\omega_T, \omega_R\} \mathbb{1}(\tau > 0), \tag{56}$$

with equality if either of the antennas are isotropic.

We remark that by symmetry, the bounds (55) and (56) hold true if we instead let position of the receiver be uniformly distributed within the room and the transmitters be fixed. Furthermore, it can be shown by some adaptation of the proof that the bound also holds in the case where both transmitter and receiver have independent and uniformly distributed but fixed orientations.

Appendix C
Deterministic Transmitter-Receiver Distance

To compute the mean arrival count for fixed transmitter-receiver distance we need to compute a conditional expectation. However, the condition renders the calculation of the mean count very cumbersome if at all possible. Instead, we approximate the expected count as motivated by the following reasoning. First, the conditional arrival count is strictly zero for $\tau < \tau_0$. Second, due to the random orientation of antennas, the direct component $\tau = \tau_0$ occurs with probability I_{LOS} defined in (16). Third, conditioning on τ_0 does not change the fact that there is exactly one mirror source per mirror room. Therefore, the mean count for $c\tau$ much greater than the diagonal of the room remains the same as in the unconditional case. Thus, we have the approximation for the conditional mean arrival count

$$\mathbb{E}[N(\tau)|\tau_0] \approx \mathbb{1}(\tau \leq \tau_0)\left(I_{\text{LOS}} + \frac{4\pi c^3(\tau^3 - \tau_0^3)\omega_T\omega_R}{3V}\right), \tag{57}$$

with corresponding conditional arrival rate

$$\lambda(\tau|\tau_0) \approx \delta(\tau - \tau_0) I_{\text{LOS}} + \mathbb{1}(\tau > \tau_0)\frac{4\pi c^3 \tau^2}{V}\omega_T\omega_R. \tag{58}$$

The right hand side of (57) coincides with that of the approximation obtained in the case with non-random transmitter and receiver location in (18). An approximation for the conditional gain $\sigma_\alpha(\tau|\tau_0)$ for $\tau > 0$ is obtained by the same line of argumentation used to derive (38). For the direct component, however, the gain obtained by inserting τ_0 in (11), and thus we obtain

$$\sigma_\alpha^2(\tau|\tau_0) \approx \begin{cases} \frac{G_T(\Omega_{T0})G_T(\Omega_{R0})}{(4\pi c\tau_0/l_c)^2}, & \tau = \tau_0 \\ \frac{\bar{g}^{\tau c S/4V}}{(4\pi c\tau/l_c)^2} \cdot \frac{1}{\omega_T\omega_R}, & \tau > \tau_0. \end{cases} \tag{59}$$

Inserting (58) and (59) into (3), we obtain the power delay spectrum

$$\begin{aligned}P(\tau|\tau_0) \approx \delta(\tau - \tau_0) I_{\text{LOS}} & \frac{G_T(\Omega_{T0})G_T(\Omega_{R0})}{(4\pi c\tau_0/l_c)^2} \\ & + \mathbb{1}(\tau > \tau_0)\frac{e^{-\tau/T}}{4\pi V/l_c^2 c}\end{aligned} \tag{60}$$

with T defined in (40).

The onset of the power delay spectrum depends on the delay of the direct component. Moreover, the onset and strength of the tail are unaffected by the transmitter and receiver positions and are thus constant throughout the whole room. For the special case of line-of-sight is known to exist, i.e. $I_{\text{LOS}} = 1$, this power delay spectrum is of the form studied in [20] and used to derive and validate distance-dependent models for the mean of the received power, mean delay and rms delay spread.

References

[1] H. Hashemi, "The indoor radio propagation channel," *Proc. IEEE*, vol. 81, no. 7, pp. 943–968, Jul. 1993.

[2] G. Turin, F. Clapp, T. Johnston, S. Fine, and D. Lavry, "A statistical model of urban multipath propagation channel," *IEEE Trans. Veh. Technol.*, vol. 21, pp. 1–9, Feb. 1972.

[3] H. Suzuki, "A statistical model for urban radio propagtion channel," *IEEE Trans. on Commun. Syst.*, vol. 25, pp. 673–680, Jul. 1977.

[4] H. Hashemi, "Simulation of the urban radio propagation," *IEEE Trans. Veh. Technol.*, vol. 28, pp. 213–225, Aug. 1979.

[5] A. A. M. Saleh and R. A. Valenzuela, "A statistical model for indoor multipath propagation channel," *IEEE J. Sel. Areas Commun.*, vol. SAC-5, no. 2, pp. 128–137, Feb. 1987.

[6] Q. H. Spencer, B. Jeffs, M. Jensen, and A. Swindlehurst, "Modeling the statistical time and angle of arrival characteristics of an indoor multipath channel," *IEEE J. Sel. Areas Commun.*, vol. 18, no. 3, pp. 347–360, 2000.

[7] T. Zwick, C. Fischer, and W. Wiesbeck, "A stochastic multipath channel model including path directions for indoor environments," *IEEE J. Sel. Areas Commun.*, vol. 20, no. 6, pp. 1178–1192, Aug. 2002.

[8] T. Zwick, C. Fischer, D. Didascalou, and W. Wiesbeck, "A stochastic spatial channel model based on wave-propagation modeling," *IEEE J. Sel. Areas Commun.*, vol. 18, no. 1, pp. 6–15, Jan. 2000.

[9] K. Haneda, J. Jarvelainen, A. Karttunen, M. Kyro, and J. Putkonen, "A statistical spatio-temporal radio channel model for large indoor environments at 60 and 70 GHz," *IEEE Trans. Antennas Propag.*, vol. 63, no. 6, pp. 2694–2704, Jun. 2015.

[10] M. K. Samimi and T. S. Rappaport, "3-D millimeter-wave statistical channel model for 5G wireless system design," *IEEE Trans on Microw. Theory and Techniques*, vol. 64, no. 7, pp. 2207–2225, Jul. 2016.

[11] M. L. Jakobsen, B. H. Fleury, and T. Pedersen, "Analysis of the stochastic channel model by Saleh & Valenzuela via the theory of point processes," in *Int. Zurich Seminar on Communications (IZS), February 29 - March 2, 2012*. Zürich, Eidgenössische Technische Hochschule Zürich, 2012.

[12] C. Holloway, M. Cotton, and P. McKenna, "A model for predicting the power delay profile characteristics inside a room," *IEEE Trans. Veh. Technol.*, vol. 48, no. 4, pp. 1110–1120, July 1999.

[13] R. Rudd and S. Saunders, "Statistical modelling of the indoor radio channel – an acoustic analogy," in *Proc. Twelfth International Conf. on Antennas and Propagation (Conf. Publ. No. 491)*, vol. 1, 31 March–3 April 2003, pp. 220–224.

[14] R. F. Rudd, "The prediction of indoor radio channel impulse response," in *The Second European Conf. on Antennas and Propagation, 2007. EuCAP 2007.*, Nov. 2007, pp. 1–4.

[15] J. B. Andersen, J. Ø. Nielsen, G. F. Pedersen, G. Bauch, and J. M. Herdin, "Room electromagnetics," *IEEE Antennas Propag. Mag.*, vol. 49, no. 2, pp. 27–33, Apr. 2007.

[16] A. Bamba, W. Joseph, J. B. Andersen, E. Tanghe, G. Vermeeren, D. Plets, J. Ø. Nielsen, and L. Martens, "Experimental assessment of specific absorption rate using room electromagnetics," *IEEE Transactions on Electromagnetic Compatibility*, vol. 54, no. 4, pp. 747–757, aug 2012.

[17] G. Steinböck, T. Pedersen, B. H. Fleury, W. Wang, and R. Raulefs, "Experimental validation of the reverberation effect in room electromagnetics," *IEEE Trans. Antennas Propag.*, vol. 63, no. 5, pp. 2041–2053, May 2015.

[18] G. Steinböck, T. Pedersen, B. Fleury, W. Wang, and R. Raulefs, "Calibration of the Propagation Graph Model in Reverberant Rooms," in *URSI Commission F Triennial Open Symposium on Radiowave Propagation and Remote Sensing*, May 2013.

[19] G. Steinböck, M. Gan, P. Meissner, E. Leitinger, K. Witrisal, T. Zemen, and T. Pedersen, "Hybrid model for reverberant indoor radio channels using rays and graphs," *IEEE Trans. Antennas Propag.*, vol. 64, no. 9, pp. 4036–4048, Sep. 2016.

[20] G. Steinböck, T. Pedersen, B. H. Fleury, W. Wang, and R. Raulefs, "Distance dependent model for the delay power spectrum of in-room radio channels," *IEEE Trans. Antennas Propag.*, vol. 61, no. 8, pp. 4327–4340, Aug. 2013.

[21] W. C. Sabine, *Collected Papers on Acoustics by Wallace Clement Sabine*. New York: Dover, 1964, originally publiced by Harvard University Press, 1922.

[22] C. F. Eyring, "Reverberation time in 'dead' rooms," *The Journal of the Acoustical Society of Amarica*, vol. 1, no. 2, p. 241, 1930.

[23] J. Kunisch and J. Pamp, "An ultra-wideband space-variant multipath indoor radio channel model," in *IEEE Conf. on Ultra Wideband Systems and Technologies, 2003*, Nov. 2003, pp. 290–294.

[24] ——, "UWB radio channel modeling considerations," in *Proc. International Conference on Electromagnetics in Advanced Applications 2003*, Turin, Sep. 2003.

[25] ——, "Measurement results and modeling aspects for the UWB radio channel," in *IEEE Conf. on Ultra Wideband Systems and Technologies, 2002. Digest of Papers*, May 2002, pp. 19–24.

[26] T. Pedersen, G. Steinböck, and B. H. Fleury, "Modeling of reverberant radio channels using propagation graphs," *IEEE Trans. Antennas Propag.*, vol. 60, no. 12, pp. 5978–5988, Dec. 2012.

[27] T. Pedersen and B. Fleury, "Radio channel modelling using stochastic propagation graphs," in *Proc. IEEE International Conf. on Commun. ICC '07*, Jun. 2007, pp. 2733–2738.

[28] T. Manabe, Y. Miura, and T. Ihara, "Effects of antenna directivity and polarization on indoor multipath propagation characteristics at 60 GHz," *IEEE J. Sel. Areas Commun.*, vol. 14, no. 3, pp. 441–448, apr 1996.

[29] N. A. Goodman and K. L. Melde, "The impact of antenna directivity on the small-scale fading in indoor environments," *IEEE Trans. Antennas Propag.*, vol. 54, no. 12, pp. 3771–3777, Dec. 2006.

[30] H. Yang, M. Herben, I. Akkermans, and P. Smulders, "Impact analysis of directional antennas and multiantenna beamformers on radio transmission," *IEEE Transactions on Vehicular Technology*, vol. 57, no. 3, pp. 1695–1707, may 2008.

[31] P. Smulders, "Statistical characterization of 60-GHz indoor radio channels," *IEEE Transactions on Antennas and Propagation*, vol. 57, no. 10, pp. 2820–2829, oct 2009.

[32] IEEE, "IEEE standard definitions of terms for antennas," *IEEE Std 145-2013 (Revision of IEEE Std 145-1993)*, pp. 1–50, March 2014.

[33] W. L. Stutzman, "Estimating directivity and gain of antennas," *IEEE Antennas and Propagation Magazine*, vol. 40, no. 4, pp. 7–11, Aug 1998.

[34] H. T. Friis, "A note on a simple transmission formula," *Proceedings of the I.R.E.*, vol. 34, no. 5, pp. 254–256, may 1946.

[35] A. Meijerink and A. F. Molisch, "On the physical interpretation of the Saleh–Valenzuela model and the definition of its power delay profiles," *IEEE Trans. Antennas Propag.*, vol. 62, no. 9, pp. 4780–4793, Sep. 2014.

[36] M. Xiao, S. Mumtaz, Y. Huang, L. Da, Y. Li, S. M. Michail Matthaiou, G. K. Karagiannidis, E. BjÃűrnson, K. Yang, C.-L. I, and A. Ghosh, "Millimeter wave communications for future mobile networks," *IEEE J. Sel. Areas Commun.*, vol. 35, no. 9, pp. 1909–1934, Sep. 2017.

[37] D. Stoyan, W. S. Kendall, and J. Mecke, *Stochastic Geometry and its Applications*, 2nd ed. John Wiley & Sons, Inc., 1995.

[38] A. Richter and R. S. Thomä, "Joint maximum likelihood estimation of specular paths and distributed diffuse scattering," in *2005 IEEE 61st Vehicular Technology Conference*, vol. 1, May 2005, pp. 11–15 Vol. 1.

[39] J. Poutanen, J. Salmi, K. Haneda, V. M. Kolmonen, F. Tufvesson, and P. Vainikainen, "Propagation characteristics of dense multipath components," *IEEE Antennas and Wireless Propagation Letters*, vol. 9, pp. 791–794, 2010.

[40] E. Leitinger, P. Meissner, C. Rüdisser, G. Dumphart, and K. Witrisal, "Evaluation of position-related information in multipath components for indoor positioning," *IEEE J. Sel. Areas Commun.*, vol. 33, no. 11, pp. 2313–2328, nov 2015.

[41] H. Kuttruff, *Room Acoustics*. London: Taylor & Francis, 2000.

[42] A. Lindau, L. Kosanke, and S. Weinzierl, "Perceptual evaluation of physical predictors of the mixing time in binaural room impulse responses," in *Audio Engineering Society Convention 128*. Audio Engineering Society, 2010.

[43] A. E. Bate and M. E. Pillow, "Mean free path of sound in an auditorium," *Proc. Physical Society*, vol. 59, pp. 535–541, 1947.

[44] R. Neubauer and B. Kostek, "Prediction of the reverberation time in rectangular rooms with non-uniformly distributed sound absorption," *Archives of Acoustics*, vol. 26, no. 3, pp. 183–201, 2001.

[45] M. Chamchoy, S. Promwong, P. Tangtisanon, and J. Takada, "Characterization of in-home uwb channel with different antenna directivity," in *2004 IEEE Region 10 Conference TENCON 2004.*, vol. C, Nov 2004, pp. 129–132 Vol. 3.

[46] J. A. Dabin, A. M. Haimovich, and H. Grebel, "A statistical ultra-wideband indoor channel model and the effects of antenna directivity on path loss and multipath propagation," *IEEE Journal on Selected Areas in Communications*, vol. 24, no. 4, pp. 752–758, April 2006.

[47] J. A. Högbom, "Aperture synthesis with a non-regular distribution of interferometer baselines," *Astronomy and Astrophysics Supplement Series*, vol. 15, no. 3, pp. 417–426, 1974.

[48] K. Sakaguchi, J. ichi Takada, and K. Araki, "On measuring the delay profile and the directions of arrival byusing super resolution algorithm," in *Proceedings of the 48th IEEE Vehicular Technology Conf.*, 1998.

[49] B. H. Fleury, M. Tschudin, R. Heddergott, D. Dahlhaus, and K. L. Pedersen, "Channel parameter estimation in mobile radio environments using the SAGE algorithm," *IEEE J. Sel. Areas Commun.*, vol. 17, no. 3, pp. 434–450, Mar. 1999.

[50] R. Thomä, M. Landmann, G. Sommerkorn, and A. Richter, "Multidimensional high-resolution channel sounding in mobile radio," in *Proc. 21st IEEE Instrumentation and Measurement Technology Conf., IMTC*, vol. 1, May 2004, pp. 257–262.